Available online at www.sciencedirect.com
ScienceDirect
Journal of Sound and Vibration 313 (2008) 29–45
JOURNAL OF SOUND AND VIBRATION
www.elsevier.com/locate/jsvi

Active control of low-frequency hull-radiated noise

Xia Pan*, Yan Tso, Ross Juniper

Maritime Platforms Division, Defence Science and Technology Organisation, P.O. Box 4331, Melbourne, Victoria 3001, Australia

Received 11 September 2006; received in revised form 20 August 2007; accepted 11 November 2007
Available online 21 December 2007

Abstract

A theoretical analysis of the active control of low-frequency radiated pressure from a finite cylindrical pressure hull is presented. The control action is implemented through a Tee-sectioned circumferential stiffener driven by a pair of PZT stack actuators. The actuators are located under the flange of the stiffener and are driven out of phase to produce a control moment. This paper examines the effects of control actions, both structurally and acoustically, for a control moment applied around the circumference of the hull. The model considered is a water-loaded finite stiffened cylindrical shell with rigid ends caps. One end of the shell is excited by an axial force while the other end is free. Control action is achieved by using the PZT actuators and stiffener to minimize the structural response and radiated pressure. It was found that the control system was capable of reducing by approximately two-thirds of the radiated pressure for the first three axial modes.

1. Introduction

The work described in this paper is concerned with the active control of the structural response and sound pressure radiation of a finite cylindrical shell subjected to an axial excitation.

Recently, the radiated pressure of a finite cylindrical shell in axisymmetric vibration has been investigated by Tso and Jenkins [1]. In their study, they simulated the response of a submarine hull due to propeller excitations as a water-loaded finite cylinder subjected to an axial force. Their model is developed for low-frequency applications such as the blade tonal noise. The active control of vibration transmission in a cylindrical shell has been studied by Pan and Hansen [2,3] using circumferential arrays of vibration control actuators and sensors. Young [4] studied the active control of vibration of an air duct using an angled stiffener and point forces. Tso and Kessissoglou [5,6] carried out an analysis of the active control of the first two structural modes of a cylindrical shell using an axial force applied at the opposite end of a primary excitation source. However, the amplitude of the axial force required was about the same order as the primary excitation, making this method impractical for real maritime structures.

The work outlined in this paper is based on the sound pressure radiation model developed by Tso and Jenkins [1] coupled with a novel active control technique where a control moment is applied to minimize the structural response and radiated pressure. The control moment is applied by using a Tee-sectioned stiffener

*Corresponding author. Tel.: +61 3 9626 8283; fax: +61 3 9626 8373.
E-mail address: xia.pan@dsto.defence.gov.au (X. Pan).

0022-460X/$ - see front matter
doi:10.1016/j.jsv.2007.11.022

Nomenclature

List of superscripts

*	complex conjugate

List of subscripts

p	plate only
c	cylindrical shell only
e	end plate only
f	primary force only
m	control moment only
c–f	cylindrical shell response due to unit primary force
c–m	cylindrical shell response due to unit control moment
p–f	plate-stiffener response due to unit primary force
p–m	plate-stiffener response due to unit control moment

combined with a pair of PZT stack actuators driven out of phase as shown in Fig. 1. Using this control strategy, the combination of the stiffener and the actuators are capable of developing a control moment of sufficient amplitude to enable the implementation of an effective control action.

2. Active control of displacement

There are two fundamental approaches considered in this paper for developing control strategies for the active control of radiated pressure from a cylindrical shell, namely, displacement control and radiated pressure control. This section describes the former approach while the latter approach is considered in the next section.

As a first approximation, the control action due to the stiffener and the stack actuators is replaced by a circumferential line moment acting around a bulkhead as shown in Fig. 2. The inclusion of the bulkhead demonstrates how the method of analysis may be applied to shells with structural discontinuities. A simplified model of the pressure hull may then be considered as a structural junction with two cylindrical shells and a

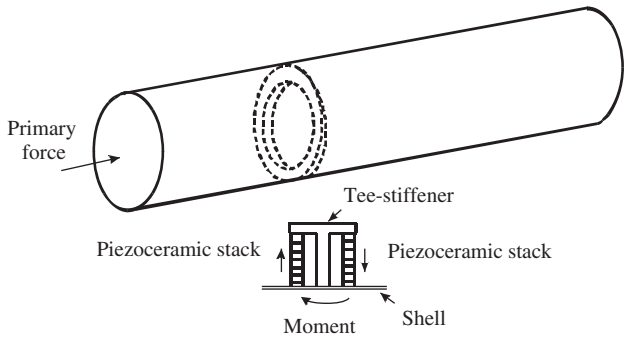

Fig. 1. Pressure hull showing primary force, control actuators and T-stiffener.

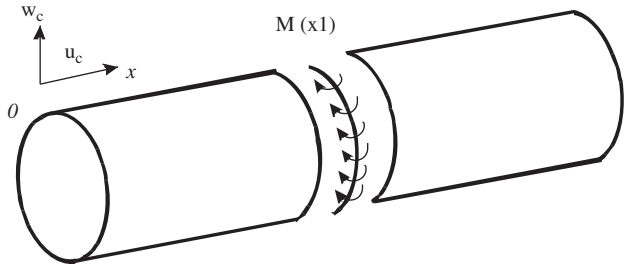

Fig. 2. Pressure hull showing line moment and plate stiffener.

circular plate. At the structural junction, both bending and in-plane waves are generated in the circular plate due to motions of the cylinder. However, in the frequency range of interest, it is thought that the predominant wave motion is bending and hence in-plane waves are ignored in the present analysis.

2.1. Analysis of the axisymmetric vibration of the pressure hull

2.1.1. Equation of motion of a cylindrical shell

The equation of motion for axisymmetric response of a ring stiffened cylindrical shell with fluid loading is given by Junger and Feit [7] and Leissa [8] as

$$\begin{bmatrix} \dfrac{\mathrm{d}^2}{\mathrm{d}x^2}+\left(1+\dfrac{m_2}{\rho_1}\right)\dfrac{\rho_1\omega^2(1-\nu^2)}{E_1h_1}, & \dfrac{\nu_1}{a}\dfrac{\mathrm{d}}{\mathrm{d}x} \\ \dfrac{\nu_1}{a}\dfrac{\mathrm{d}}{\mathrm{d}x}, & \dfrac{1}{a^2}+\dfrac{A_r(1-\nu_1^2)}{ba^2h_1}+\alpha^2\beta^2\dfrac{\mathrm{d}^4}{\mathrm{d}x^4}-\left(1+\dfrac{m_1}{\rho_1}\right)\dfrac{\rho_1\omega^2(1-\nu_1^2)}{E_1h_1} \end{bmatrix}, \begin{bmatrix} u_c \\ w_c \end{bmatrix} = \begin{bmatrix} 0 \\ 0 \end{bmatrix}, \tag{1}$$

where a is the radius of shell (m), A_r the cross-sectional area of stiffener (m^2), b the stiffener spacing (m), E_1 the Young's modulus (N/m^2), h_1 the shell thickness (m), m_1 the fluid loading parameter (kg/m^2), m_2 the equivalent distributed mass of the internal structure and on-board equipment (kg/m^2), $\beta^2=(h_1^2/12a^2)$, ν_1 the Poisson's ratio, ρ_1 the mass per unit area of the stiffened shell (kg/m^2), ρ_f the density of fluid (kg/m^2) and ω the circular frequency (rad/s).

The complete solution of the cylindrical shell is

$$u_c=\sum_{i=1}^{6} W_{ci}C_i\mathrm{e}^{\lambda_i x/a} \tag{2}$$

and

$$w_c=\sum_{i=1}^{6} W_{ci}\mathrm{e}^{\lambda_i x/a}, \tag{3}$$

where λ_i, $i=1,2,\ldots,6$ are the wave numbers. The amplitude ratios C_i, $i=1,2,\ldots,6$ are given by Tso and Jenkins [1] as

$$C_i=\frac{U_{ci}}{W_{ci}}=\frac{-\nu\lambda_i}{\lambda_i^2+\varpi\Omega^2}, \tag{4}$$

where

$$\Omega^2=\frac{\omega^2a^2\rho_1(1-\nu_1^2)}{E_1h_1} \tag{5}$$

and

$$\varpi=1+\frac{m_2}{\rho_1}. \tag{6}$$

Wave amplitudes W_i, $i=1,2,\ldots,6$ may be determined from the boundary conditions of the cylinder [1].

2.1.2. Equation of motion of a circular plate in bending motion

The equation of motion of a circular plate in bending motion is given by Leissa [9] as

$$\nabla^4\omega_p+\left[\frac{12\rho_p\omega^2(1-\upsilon_p^2)}{E_ph_p^2}\right]w_p=0, \tag{7}$$

where E_p is the Young's modulus of plate (N/m^2), h_p the plate thickness (m), r_p the radius of plate (m), w_p the out-of-plane plate displacement (m), ρ_p the density of plate (kg/m^3) and υ_p the Poisson's ratio of plate:

$$\nabla^4 = \left[\frac{\mathrm{d}^2}{\mathrm{d}r_p^2} + \frac{1}{r_p}\frac{\mathrm{d}}{\mathrm{d}r_p}\right]^2.$$

Laplacian operator for axisymmetric motion.

The solution to Eq. (7) may be obtained in terms of the Bessel functions:

$$w_p = B_1 J_0(k_p r_p) + B_2 I_0(k_p r_p), \tag{8}$$

where the plate bending wave number $k_p = [12\rho_p\omega^2(1-\upsilon_p^2)/E_p h_p^2]^{1/4}$, J_0 and I_0 are Bessel function of the first kind and modified Bessel functions of the first kind, respectively, and B_1 and B_2 are constants to be determined from the boundary conditions. It is assumed that the circular plate does not impose any in-plane constraint on the cylinder.

2.2. Expressions for forces and moments

Consider the structural junction between two cylinder segments (1) and (2) as shown in Fig. 3, the junction forces and moments are given by Leissa [8,9] as

$$F_x = \frac{-E_1 h_1}{1-v_1^2}\left(\frac{\mathrm{d}u_c}{\mathrm{d}x} + \frac{\upsilon_1}{a}w_c\right)_{x=x_1}, \tag{9}$$

$$F_z = \frac{E_1 h_3}{12(1-v_1^2)}\left(\frac{\mathrm{d}^3 w_c}{\mathrm{d}x^3}\right)_{x=x_1}, \tag{10}$$

$$M = \frac{-E_1 h_1^3}{12(1-v_1^2)}\left(\frac{\mathrm{d}^2 w_c}{\mathrm{d}x^2}\right)_{x=x_1}, \tag{11}$$

$$F_p = \frac{E_p h_p^3}{12(1-v_p^2)}\left(\frac{\mathrm{d}^3 w_p}{\mathrm{d}r_p^3} + \frac{1}{r_p}\frac{\mathrm{d}^2 w_p}{\mathrm{d}r_p^2} - \frac{1}{r_p^2}\frac{\mathrm{d}w_p}{\mathrm{d}r_p}\right)_{r_p=a} \tag{12}$$

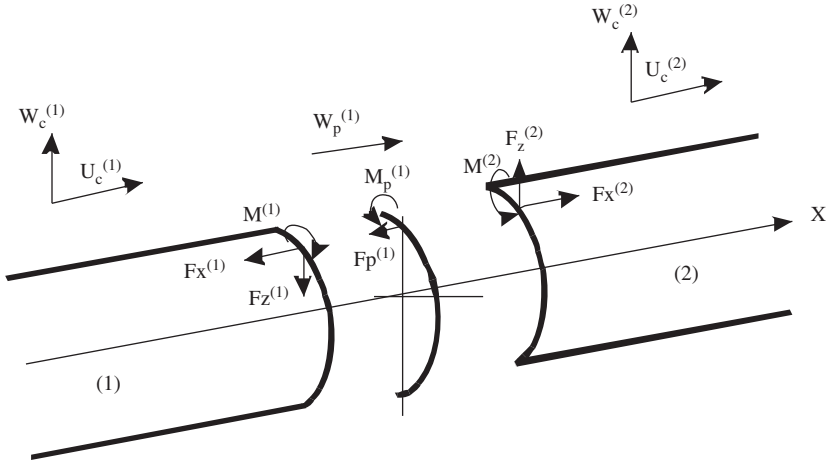

Fig. 3. Junction forces and moments.

and

$$M_p = \frac{-E_p h_p^3}{12(1-v_p^2)}\left(\frac{\mathrm{d}^2 w_p}{\mathrm{d}r_p^2} + \frac{\upsilon_p}{r_p}\frac{\mathrm{d}w_p}{\mathrm{d}r_p}\right)_{r_p=a}. \tag{13}$$

2.3. Solution of the dynamic response of the pressure hull

Referring to Figs. 3 and 2, the equilibrium conditions at $x = x_1$ require

$$F_x^{(1)} + F_p^{(1)} - F_x^{(2)} = 0, \tag{14}$$

$$F_z^{(1)} - F_z^{(2)} = 0, \tag{15}$$

$$M^{(1)} - M_p^{(1)} - M^{(2)} = M_c, \tag{16}$$

where M_c is the control moment.

The compatibility of junction displacements requires

$$u_c^{(1)} = u_c^{(2)}, \tag{17}$$

$$u_c^{(1)} = w_p^{(1)}, \tag{18}$$

$$w_c^{(1)} = w_c^{(2)}, \tag{19}$$

$$\frac{\mathrm{d}w_c^{(1)}}{\mathrm{d}x} = \frac{\mathrm{d}w_c^{(2)}}{\mathrm{d}x}, \tag{20}$$

$$\frac{\mathrm{d}w_c^{(1)}}{\mathrm{d}x} = -\frac{\mathrm{d}w_p^{(1)}}{\mathrm{d}r_p}. \tag{21}$$

The following boundary conditions are applicable to a finite cylinder with rigid end plates.

At $x = 0$,

$$\frac{\mathrm{d}w_c^{(1)}}{\mathrm{d}x} = 0, \tag{22}$$

$$\frac{F}{2\pi a} - F_x^{(1)} - \frac{m^{(0)}}{2\pi a}\frac{\mathrm{d}^2 u_c^{(1)}}{\mathrm{d}t^2} = 0 \tag{23}$$

and

$$w_c^{(1)} = 0. \tag{24}$$

At $x = L$,

$$w_c^{(2)} = 0, \tag{25}$$

$$\frac{\mathrm{d}w_c^{(2)}}{\mathrm{d}x} = 0 \tag{26}$$

and

$$F_x^{(2)} - \frac{m^{(L)}}{2\pi a}\frac{\mathrm{d}^2 u_c^{(2)}}{\mathrm{d}t^2} = 0, \tag{27}$$

where $m^{(0)}$ and $m^{(L)}$ are the masses of the end plates at $x = 0$ and L, respectively.

The end conditions of the cylinder (Eqs. (22)–(27)), together with the boundary conditions for a cylinder/plate junction (Eqs. (14)–(21)), provide sufficient conditions for the solution of the cylindrical hull and end plates.

If the pressure hull is excited by a sinusoidal axial force of amplitude F located at $x = 0$, the flexural displacement $w_c(x)$ at any location x may be expressed as

$$w_c(x) = Fw_{c-f}(x), \tag{28}$$

where w_{c-f} is the flexural displacement per unit axial force.

Similarly, if a line moment of amplitude M is applied at $x = x_1$, the flexural displacement due to this moment is

$$w_c(x) = Mw_{c-m}(x), \tag{29}$$

where w_{c-m} is the flexural displacement per unit line moment.

The total flexural displacement at x due to the primary and control excitations together is then

$$w_c(x) = Fw_{c-f}(x) + Mw_{c-m}(x). \tag{30}$$

The optimal moment which minimizes the flexural displacement at $x = x_e$ is obtained from Eq. (30) by setting $w_c(x_e)$ to be zero, i.e.,

$$M = -F\frac{w_{c-f}(x_e)}{w_{c-m}(x_e)}. \tag{31}$$

Similarly, the optimal moment which minimizes the axial displacement at x_e is

$$M = -F\frac{u_{c-f}(x_e)}{u_{c-m}(x_e)}, \tag{32}$$

where u_{c-f} is the axial displacement per unit primary force and u_{c-m} is the axial displacement per unit control line moment.

The optimal control moment for minimizing both radial spectral displacement (defined in Eq. (37) in Appendix A) and axial displacement may be found by evaluating the sum of the squares of each displacements and setting the result to zero.

3. Active control of sound radiation

The total sound radiation of a pressure hull may be considered as the sum of the pressure due to the end plates and the radial motion of the cylinder (see Appendix A). The pressure due to the radial motion of the

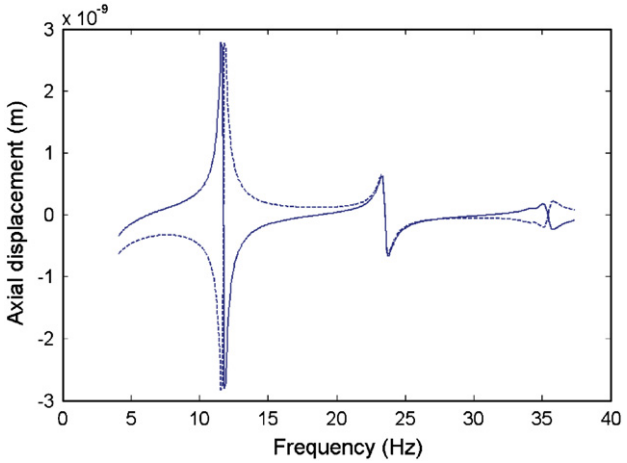

Fig. 4. Axial response of the pressure hull. —, axial displacement at $x = 0$, - - -, axial displacement at $x = L$.

primary and control excitation together is

$$p_c(R,\theta) = Fp_{c-f}(R,\theta) + Mp_{c-m}(R,\theta), \tag{33}$$

where p_{c-f} is the pressure due to a unit primary force excitation and p_{c-m} is the pressure due to a unit control moment excitation. Similarly, the pressure due to the end plates can be shown as

$$p_e(R,\theta) = Fp_{e-f}(R,\theta) + Mp_{e-m}(R,\theta), \tag{34}$$

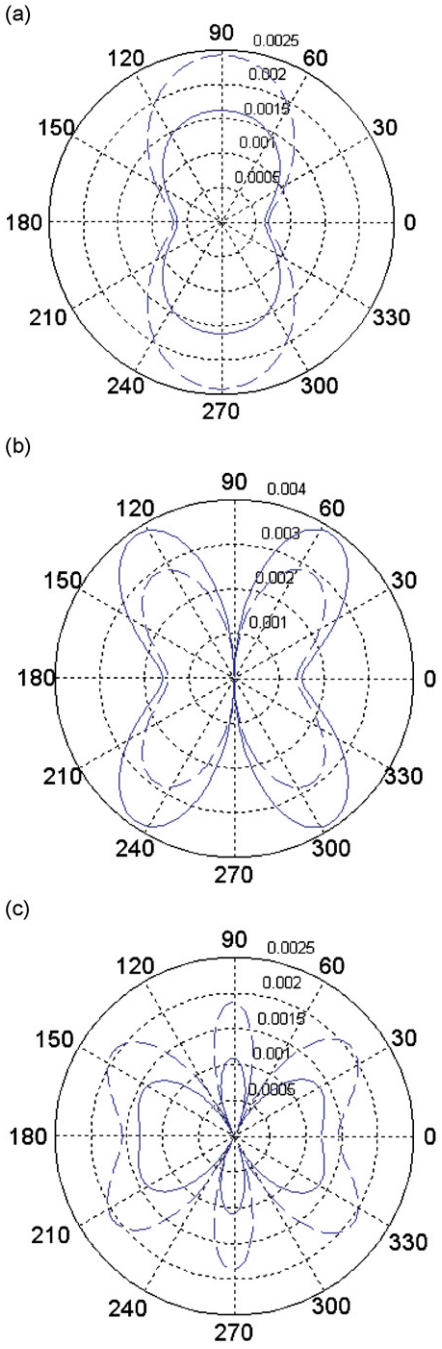

Fig. 5. Radiated pressure: (a) at first mode; (b) at second axial mode; (c) at third axial mode. —, total pressure; – – –, radiation due to end plates. In this and other figures, the radiated pressure is plotted in polar coordinate with angle in degrees and radius in Pascals.

where p_{e-f} is the axial pressure due to a unit primary force excitation and p_{e-m} is the axial pressure due to a unit control moment excitation.

The total sound radiation then becomes

$$p_{\text{tot}} = \int_0^{2\pi} p_c(R,\theta)\,\mathrm{d}\theta + \int_0^{2\pi} p_e(R,\theta)\,\mathrm{d}\theta$$
$$= F\int_0^{2\pi} [p_{c-f}(R,\theta) + p_{e-f}(R,\theta)]\,\mathrm{d}\theta + M\int_0^{2\pi} [p_{c-m}(R,\theta) + p_{e-m}(R,\theta)]\,\mathrm{d}\theta. \quad (35)$$

The optimal control moment to minimize the total radiated pressure is obtained by determining the derivatives of Eq. (35) with respect to the control moment and setting the result to zero. The optimal control moment may then be expressed as

$$M = -F\frac{\int_0^{2\pi}[p_{c-f}(R,\theta) + p_{e-f}(R,\theta)][p_{c-m}(R,\theta) + p_{e-m}(R,\theta)]^*\,\mathrm{d}\theta}{\int_0^{2\pi} |p_{c-m}(R,\theta) + p_{e-m}(R,\theta)|^2\,\mathrm{d}\theta}. \quad (36)$$

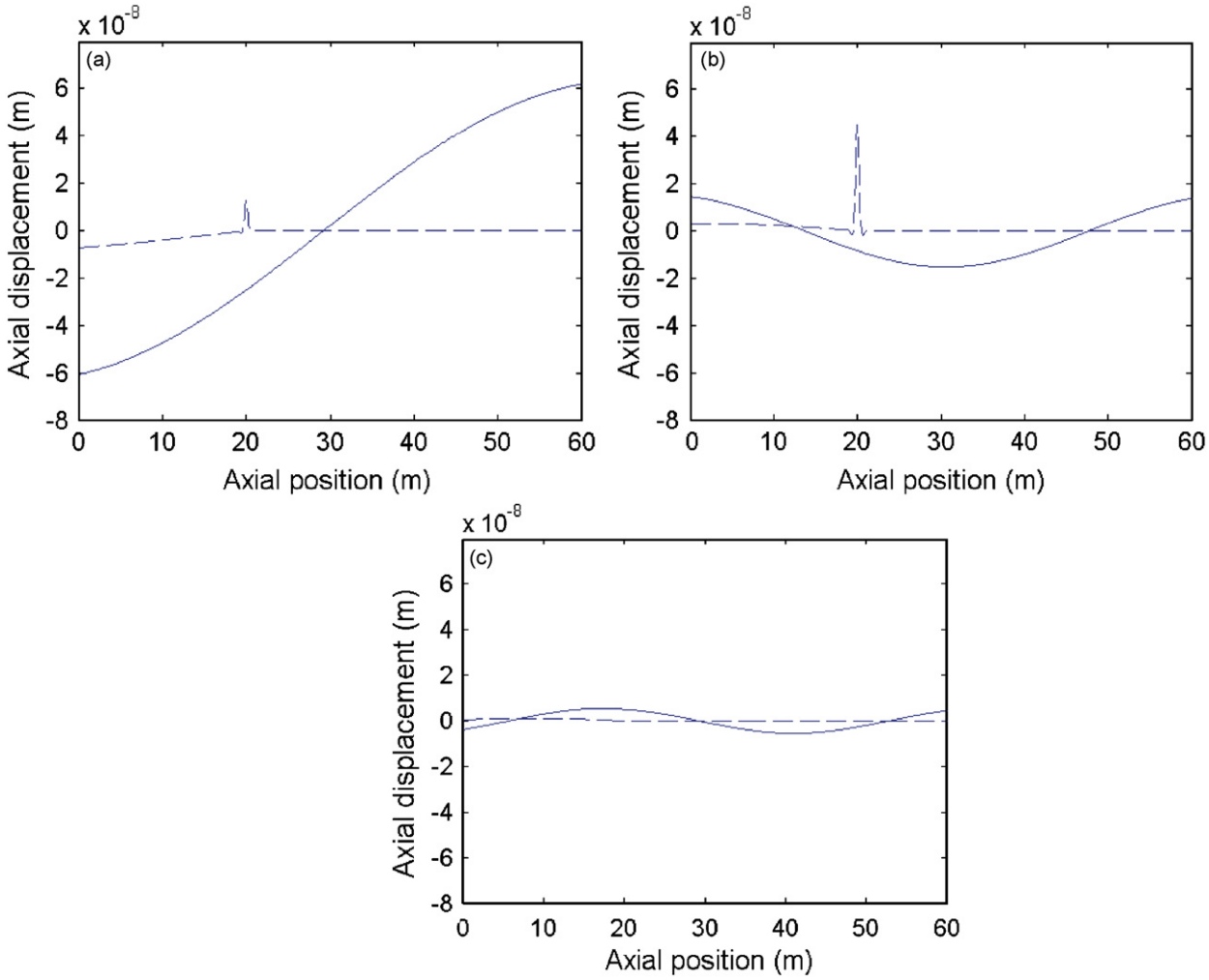

Fig. 6. Axial displacement with the control moment (line moment) using axial displacement as the cost function: (a) at first mode; (b) at second axial mode; (c) at third axial mode. —, uncontrolled; - - -, controlled.

4. Numerical results

The numerical results presented in this section were based on a steel pressure hull of 7 m diameter, 60 m length and a shell thickness of 25 mm. A primary excitation force of 1 N amplitude is applied at $x = 0$ m and the control moment at $x = 20$ m. The sound pressure level at a distance of 1000 m is used as the error signal for sound radiation control. Additional results are presented in Section 4.3 for other control source locations.

Fig. 4 shows the axial displacement at both ends of the pressure hull as a function of frequency. In order to obtain realistic amplitudes near the resonant frequency of the hull, a structural loss factor of 0.02 is used in the calculations. It can be seen that the first three axial modes are approximately 12, 24 and 35 Hz.

Fig. 5 shows the total radiated pressure for the first three axial modes. The radiated pressure due to the end plates only is also shown in the figures for comparison. The figures show that for the first and third modes, the radiated pressure due to the radial motion of the cylinder is out of phase with that of the axial motion, resulting in a reduction of the total radiated sound pressure. It is therefore important to account for the phase difference between the axial motion of the end plates and the radial motion of the cylinder in the analysis of cylinder radiation.

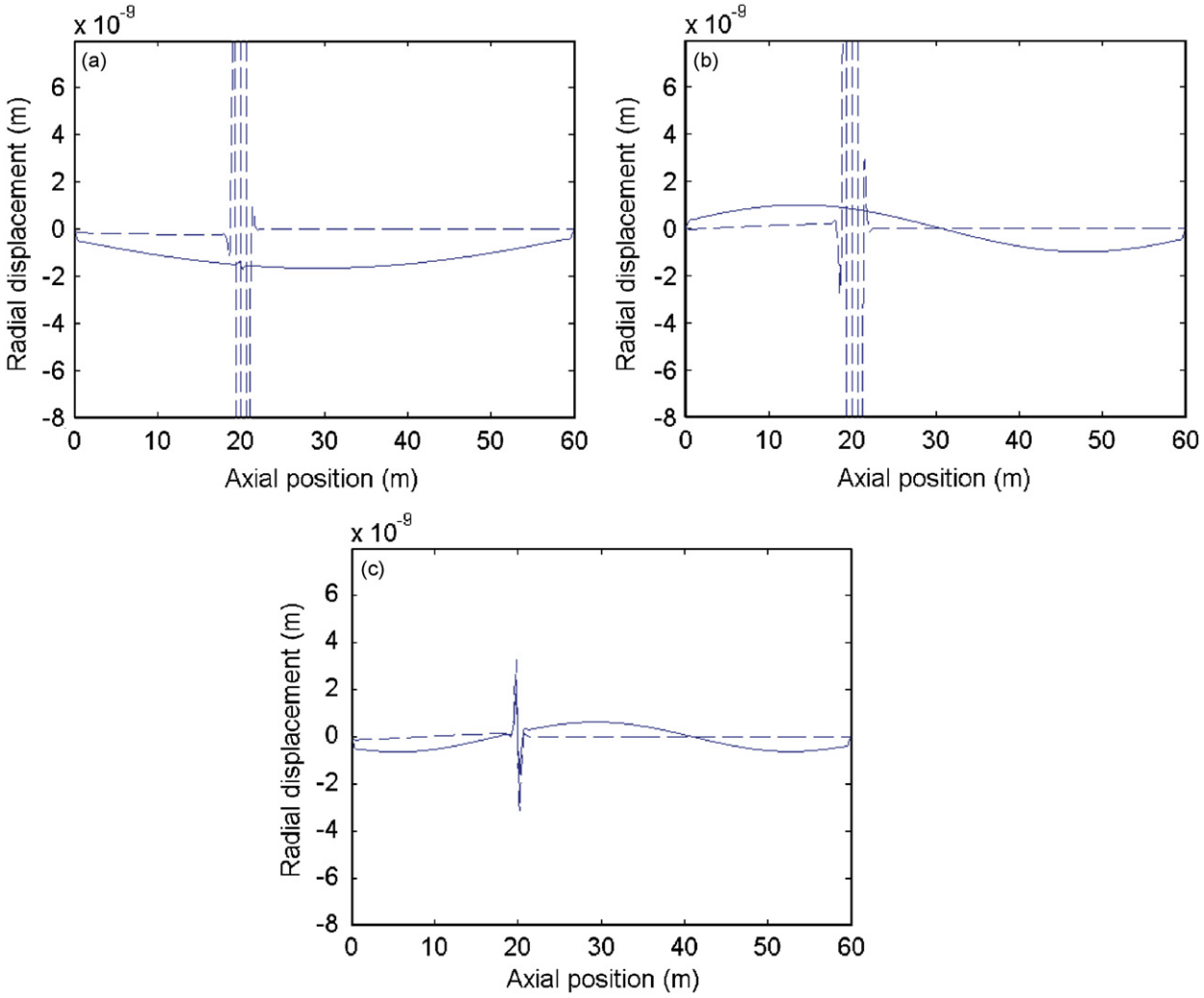

Fig. 7. Radial displacement with the control moment (line moment) using axial displacement as the cost function: (a) at first mode; (b) at second axial mode; (c) at third axial mode. —, uncontrolled; - - -, controlled.

4.1. Minimization of displacement

The first control strategy to be investigated in this section is the minimization of displacement at the end plates. Fig. 6 shows the controlled and uncontrolled mode shapes of the first three axial hull modes. The phase relationship between the ends of the pressure hull can clearly be observed. The results demonstrate that the axial displacement at the ends of the hull is reduced significantly for the first three axial modes.

However, in order to minimize the axial motion of the end plates, the control actuators have to induce a significant radial motion on the cylinder. Fig. 7 shows the controlled and uncontrolled radial displacement for the first three hull modes. With the application of control actions, large radial displacements at the actuator location can be observed for the first two modes (see Fig. 7(a and b)), and to a lesser extent for the third mode (see Fig. 7(c)).

The effect of the controlled radial displacement (presented in Fig. 7) on the total radiated pressure is shown in Fig. 8. It can be seen that, for the first two axial modes (Fig. 8(a and b)), the total radiated pressure with displacement control is very much higher than the uncontrolled case due to the large radial displacements. For the third axial mode (Fig. 8(c)), the total radiated pressure with displacement control is reduced, as the small increase in radial displacement is more than compensated by the significant reduction of axial displacement (see Figs. 6(c) and 7(c)).

Another cost function that has been evaluated in this section is the radial spectral displacement of the cylindrical shell (see Eq. (37) in Appendix A for an expression of the radial spectral displacement). Fig. 9 shows the controlled and uncontrolled radiated pressure for the first three axial modes. It can be seen that the radiated pressure is increased with the application of control action for the first axial mode while no significant difference is observed for the second and third modes. The results suggest that the control action in itself will

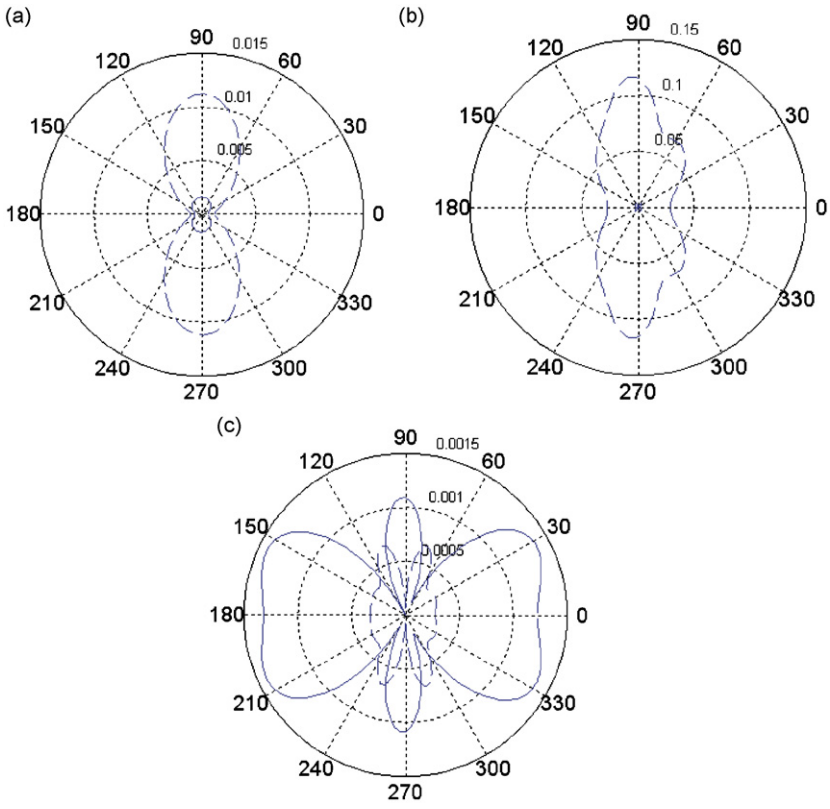

Fig. 8. Total radiated pressure with the control moment (line moment) using axial displacement as the cost function: (a) at first mode; (b) at second axial mode; (c) at third axial mode. —, uncontrolled; - - -, controlled.

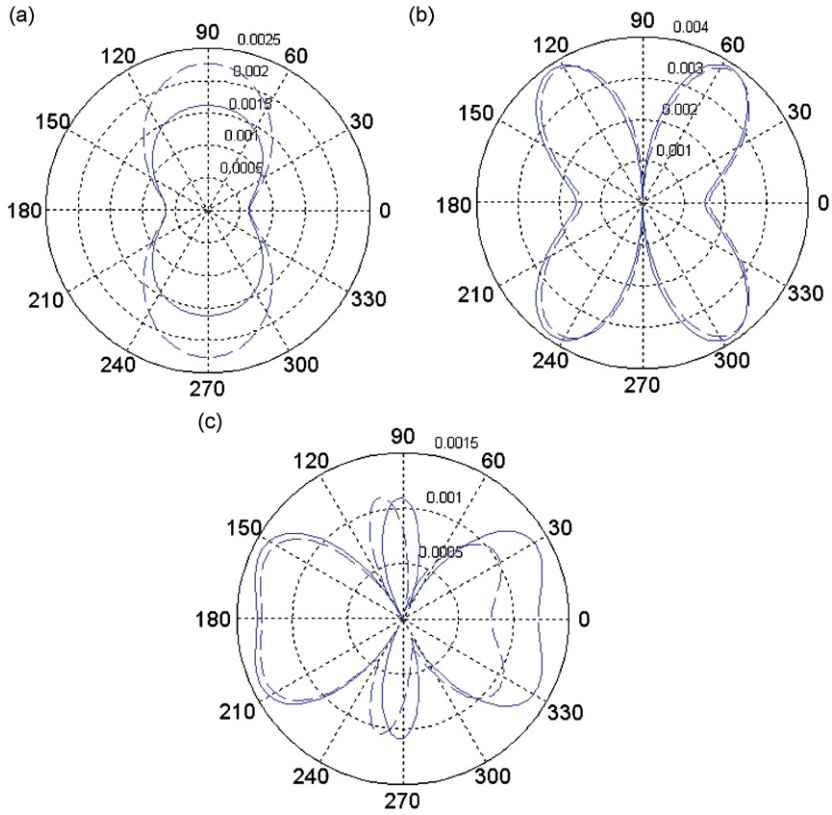

Fig. 9. Total radiated pressure with the control moment (line moment) using radial spectral displacement as the cost function: (a) at first mode; (b) at second axial mode; (c) at third axial mode. —, uncontrolled; - - -, controlled.

introduce a radial displacement which renders this control strategy ineffective. Also, a radial motion will give rise to an axial displacement and further reduces the effectiveness of the control action.

Finally, the sum of the axial displacement and the radial spectral displacement is used as the cost function for minimization. Fig. 10 shows the radiated pressure for the controlled and uncontrolled cases. In general, this control strategy is not effective in controlling the radiated pressure, as can be seen from the results for the first and second axial modes. This is partially due to the coupling between the radial and axial displacements of the cylinder which results in a significant pressure radiation from these motions. Also, this cost function does not include the areas of the cylindrical shell and the end plates which may have an effect on the appropriate weighting and hence the level of reduction of the radiated pressure.

The results presented in this section suggest that a different cost function is warranted to account for the axial modes of interest.

4.2. Minimization of radiated pressure

The cost function to be minimized in this control strategy is the total radiated pressure. This method of control may be implemented by an array of accelerometers to measure the radial motion of the shell in order to determine the component of radiated pressure due to the radial motion (refer to the acceleration measurement system in Ref. [4]). The component of radiated pressure due to axial motion may be determined by measuring the displacement of the end plates.

Fig. 11(a) shows the controlled and uncontrolled total radiated pressure at the first axial mode by minimizing the radiated pressure at 90° from the cylinder axis, where the control action is more effective in this orientation. It can be observed that approximately two-thirds of the total pressure has been reduced.

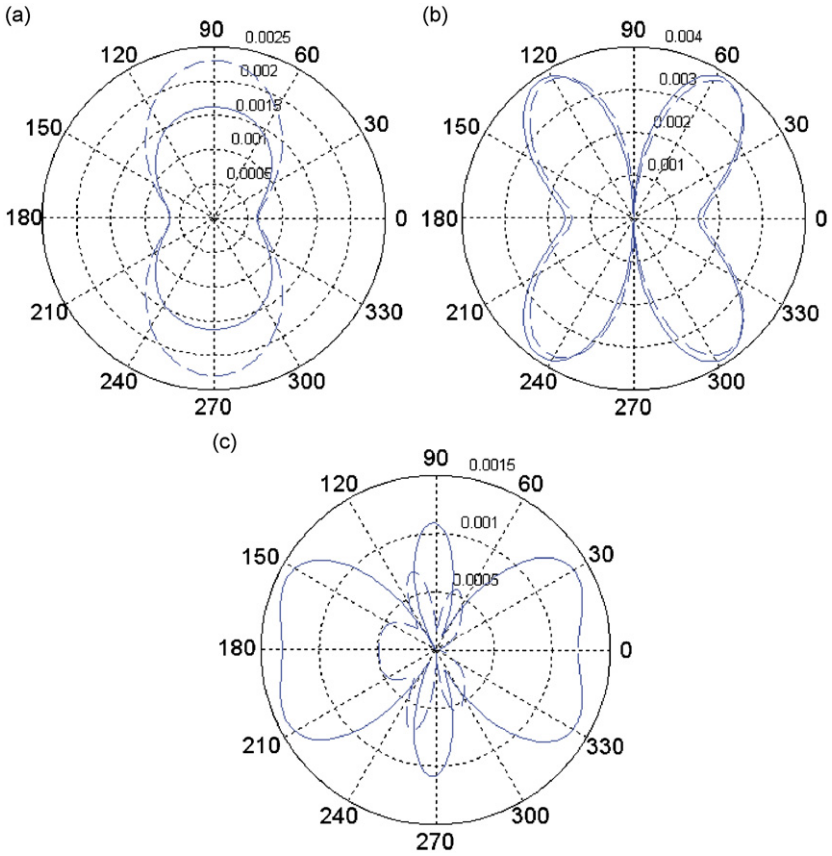

Fig. 10. Total radiated pressure with the control moment (line moment) using the sum of mean squared radial spectral displacement and axial displacement as the cost function: (a) at first mode; (b) at second axial mode; (c) at third axial mode. —, uncontrolled; - - -, controlled.

Fig. 11(b and c) shows the results for the second and third modes, respectively. The results were obtained by minimizing the sum of the total radiated pressure from 0° to 180°. Again, a significant reduction of radiation pressure can be observed.

By comparing the results between Figs. 10 and 11, it can be seen that the radiated pressure is a more effective cost function than displacement for this control configuration.

The moment location and the ratio between the amplitude of the control moment and primary force (see Eq. (36)) are presented in Table 1. It shows that the amplitude of the control moment is much lower than the primary force for the first three axial modes. To put these figures into perspective, a typical PZT stack can generate a pushing force of 30 kN. By placing the stacks under a 200 mm flange (with a moment arm of 100 mm), it translates to a point moment of 3 kN m. If the PZT stacks are spaced at 500 mm interval around the circumference of the hull, it will give an equivalent line moment of 6 kN m/m. Referring back to Table 1, a control moment of 6 kN m/m is capable of controlling a primary force of 40 kN for the first axial mode which is sufficient for marine applications. Based on the specifications from manufacturers of the stack actuator and power amplifier, the electrical power requirement for such a control system would be approximately 5 kW, which is feasible for installation in marine vessels.

4.3. Effect of stiffener and control actuator location

In practice, it may not be feasible to locate the control actuators at a specific position along the cylindrical shell, say at $L/3$, and a physically convenient location may not be optimum for the attenuation of

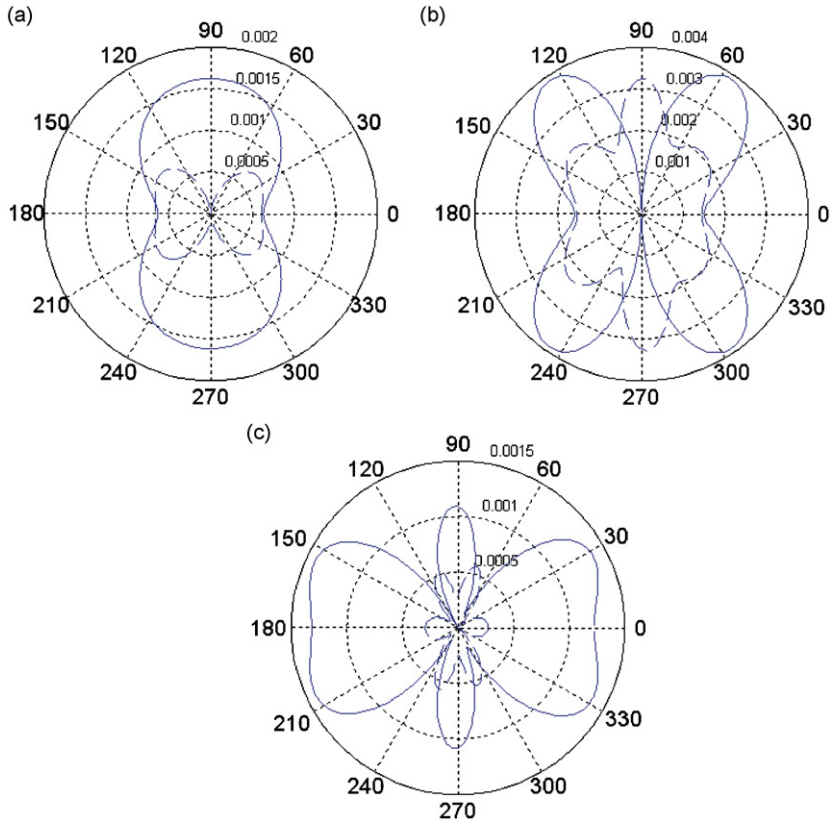

Fig. 11. Total radiated pressure with the control moment (line moment) using pressure as the cost function: (a) at first mode; (b) at second axial mode; (c) at third axial mode. —, uncontrolled; - - -, controlled.

Table 1
Line moment location and moment/force ratio

Axial mode	Location of moment (m)	Moment/force ratio
First mode	20	0.15
Second mode	20	0.16
Third mode	20	0.008

noise radiation. This section explores the effect of locating the control actuator at other positions on noise radiation.

In order to implement an effective control of the total radiated pressure, calculations were conducted with actuator locations at 1 m increments along the length of the cylindrical shell. It was found that the control actuator should be located close to the primary source for optimum attenuation. This enables an effective control of the motion at the other end without causing an excessive radial motion.

Table 2 shows the locations of the control actuator and the amplitude ratio between the control moment and primary force. Again, the amplitude of the control moments is much lower than the primary force.

Fig. 12 shows the total radiated pressure of the first three modes that corresponds to the control actuator locations as shown in Table 2. The radiation pattern of the second mode (Fig. 12(b)) differs considerably from Fig. 11(b) due to the difference in location of the actuator. Also, a larger attenuation is achieved with the control moment located close to the excitation source. Both the first and third modes (Fig. 12(a and c)) show

Table 2
Line moment location and moment/force ratio with the control moment close to the excitation source

Axial mode	Location of moment (m)	Moment/force ratio
First mode	0.25	0.13
Second mode	0.25	0.12
Third mode	0.25	0.007

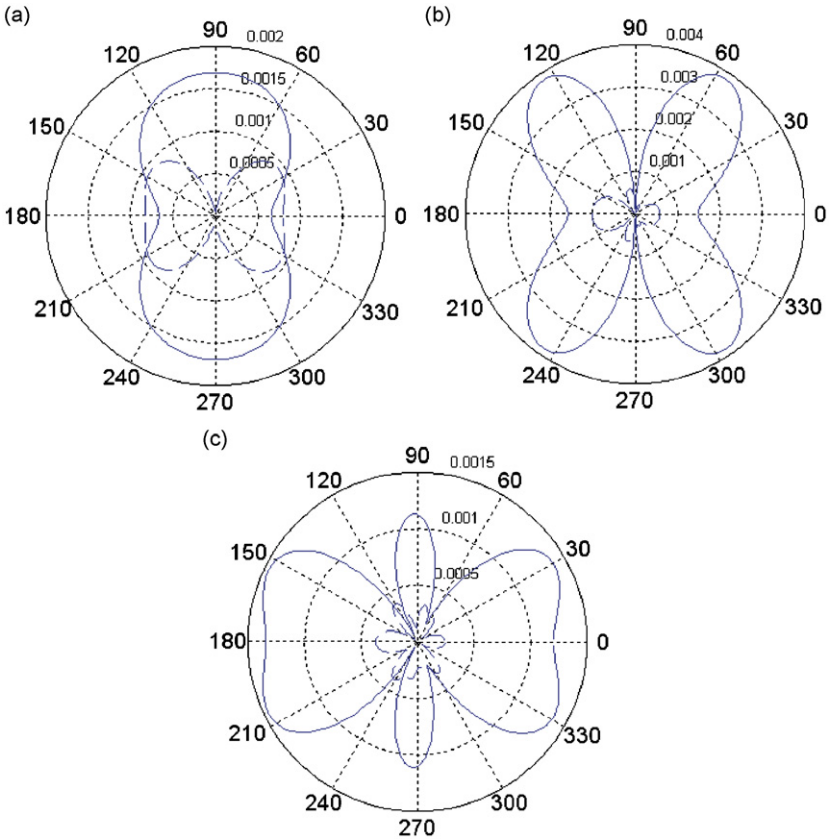

Fig. 12. Total radiated pressure with the control moment (line moment) close to the excitation source using pressure as the cost function: (a) at first mode; (b) at second axial mode; (c) at third axial mode. —, uncontrolled; - - -, controlled.

similar reduction in radiated pressure compared with Fig. 11(a and c). It seems that the second mode is more sensitive to the control moment location for this control configuration.

4.4. Comparison between line moment control and point moment control

The implementation of the control system requires a series of point moments to be applied around the circumference of the hull. To investigate the effect of replacing a line moment with a series of point moments, calculations were performed for the total radiated pressure of the first three modes with the actuator locations shown in Table 2, but in this case the system is controlled by three evenly spaced equivalent point moments. Fig. 13 presents the results of these calculations. It can be seen that the results are very similar to those of line moment control and therefore in practical terms, point moments may be used without reducing the effectiveness of the control action.

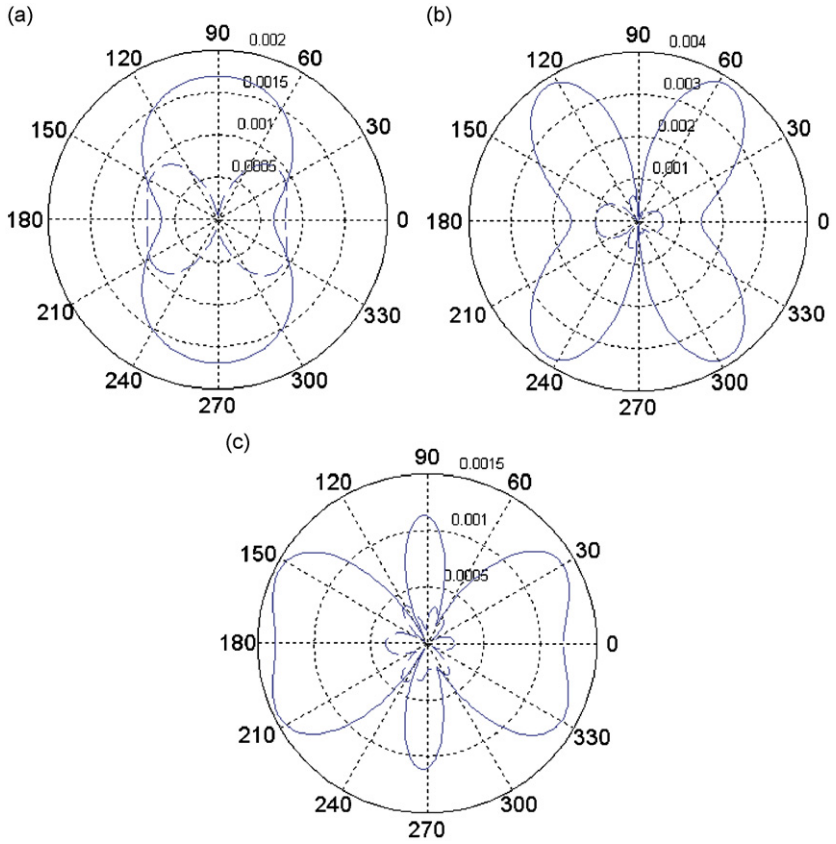

Fig. 13. Total radiated pressure with the control moment (three point moments) close to the excitation source using pressure as the cost function: (a) at first mode; (b) at second axial mode; (c) at third axial mode. —, uncontrolled; - - -, controlled.

5. Conclusions

The radiated pressure of a cylindrical shell subjected to an axial excitation may be reduced by approximately two-thirds using an active control moment. The amplitude of the control moment is small compared with the excitation force and may be implemented by a series of PZT stack actuators.

The most effective cost function for the control system is the radiated pressure. This control strategy requires a number of sensors to measure the structural response of the pressure hull and an accurate model to predict the radiated noise. An alternative control strategy is the minimization of the axial displacement which may reduce the radiated pressure for higher order axial modes. However, at the first and second modes, the control of axial motion may lead to a higher overall radiated pressure due to the large radial motion. This finding indicates that the phasing between the radial and axial motions is a significant factor in the application of active control to reduce the radiated pressure.

Appendix A

A.1. The radiation of sound from the cylindrical surface

The far field pressure due to axisymmetric vibration of a cylindrical shell shown in Fig. 14 is given by Junger and Feit [7] and later used by Tso and Jenkins [1]:

$$p_c(R,\theta) = \frac{\mathrm{j}\rho_f \omega^2 \mathrm{e}^{\mathrm{j}k_f R} w_c(k_f \cos\theta)}{\pi k_f R \sin\theta H_1(k_f a \sin\theta)}, \tag{37}$$

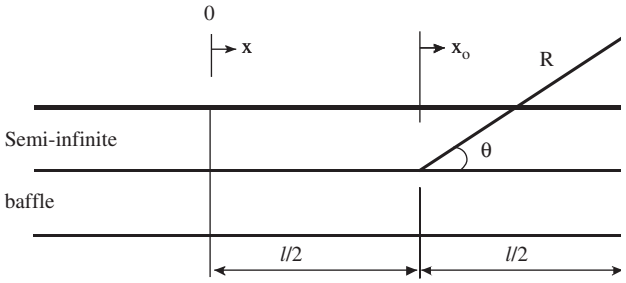

Fig. 14. Finite cylindrical shell with semi-infinite baffles.

where $w_c(k_f \cos\theta)$ is spectral displacement evaluated at $k_f \cos\theta$ and is defined as

$$w_c(k_f \cos\theta) = \int_{-L/2}^{L/2} w_c(x) e^{-jk_f \cos\theta x}\, dx.$$

$H_1(k_f \sin\theta)$ is the Hankel function of order 1.

A.2. Radiation from the end plates

The pressure field due to the rigid end plates given by Tso and Jenkins [1] is

$$p_e(R) = B_{p1}B_{u1}\ddot{v}_1 + B_{p2}B_{u2}\ddot{v}_2, \tag{38}$$

where v_1 and v_2 are the displacements of two end plates, and B_{p1}, B_{p2}, B_{u1} and B_{u2} are given by Tso and Jenkins [1] as

$$B_{p1} = \rho_f \left[\frac{j}{k_f}(e^{jk_f a} - 1)\left(jk_f - \frac{1}{R}\right)\cos\theta - 1\right], \tag{39}$$

$$B_{p2} = \rho_f \left[\frac{j}{k_f}(e^{jk_f a} - 1)\left(jk_f - \frac{1}{R}\right)\cos\theta + 1\right], \tag{40}$$

$$B_{u1} = \frac{-aJ_1(k_f a \sin\theta)e^{jk_f[R-(L/2)\cos\theta]}}{2Rk_f \sin\theta}, \tag{41}$$

$$B_{u2} = \frac{-aJ_1(k_f a \sin\theta)e^{jk_f[R+(L/2)\cos\theta]}}{2Rk_f \sin\theta}. \tag{42}$$

References

[1] Y.K. Tso, C.J. Jenkins, Low Frequency Hull Radiation Noise, Report No. Dstl/TR05660, Defence Science and Technology Laboratory, UK, 2003.
[2] X. Pan, C.H. Hansen, Active control of vibration transmission in a cylindrical Shell, *Journal of Sound and Vibration* 203 (1997) 409–433.
[3] X. Pan, C.H. Hansen, An experimental study of active control of vibration transmission in a cylindrical shell, *Proceedings of the 131st Meeting of the Acoustic Society of America*, Indianapolis, USA, 1996.
[4] A.J. Young, Active Control of Vibration in Stiffened Structures, PhD Thesis, University of Adelaide, 1995, pp. 156–234.
[5] Y.K. Tso, N. Kessissoglou, C. Norwood, Active control of a fluid-loaded cylindrical shell, part 1: dynamics of the physical system. *Proceedings of the Eighth Western Pacific Acoustics Conference*, Melbourne, Australia, 2003.
[6] N. Kessissoglou, Y.K. Tso, C. Norwood, Active control of a fluid-loaded cylindrical shell, part 2: active modal control, *Proceedings of the Eighth Western Pacific Acoustics Conference*, Melbourne, Australia, 2003.

[7] M.C. Junger, D. Feit, *Sound, Structures, and their Interaction*, MIT Press, Cambridge, MA, 1985.
[8] A.W. Leissa, *Vibration of Shells*, National Aeronautics and Space Administration, Washington, DC, 1973, pp. 1–184.
[9] A.W. Leissa, *Vibration of Plates*, National Aeronautics and Space Administration, Washington, DC NASA Special Report 160, 1969.